Design and analysis of high-gain DC–DC chopper topologies for PV-fed BLDC motor drive system

Zakaria Mohamed Salem Elbarbary
Department of Electrical Engineering, King Khalid University, Abha, Saudi Arabia
Ahmed A. Alaifi
Department of Electrical Technology, College of Technology, Abha, Saudi Arabia
Saad Fahed Alqahtani
Department of Electrical Engineering, King Khalid University, Abha, Saudi Arabia
Irshad Mohammad Shaik
College of Engineering, King Khalid University, Abha, Saudi Arabia
Sunil Kumar Gupta
Department of Electrical and Electronics Engineering, Jaipur Engineering College and Research Centre, Jaipur, India, and
Vijayakumar Gali
School of Engineering and Digital Sciences, Nazarbayev University, Astana, Kazakhstan

Received 4 April 2023
Revised 9 May 2023
19 May 2023
Accepted 25 May 2023

Abstract

Purpose – Switching power converters for photovoltaic (PV) applications with high gain are rapidly expanding. To obtain better voltage gain, low switch stress, low ripple and cost-effective converters, researchers are developing several topologies.

Design/methodology/approach – It was decided to use the particle swarm optimization approach for this system in order to compute the precise PI controller gain parameters under steady state and dynamic changing circumstances. A high-gain q- ZS boost converter is used as an intermittent converter between a PV and brushless direct current (BLDC) motor to attain maximum power point tracking, which also reduces the torque ripples. A MATLAB/Simulink environment has been used to build and test the positive output quadratic boost high gain converters (PQBHGC)-1, PQBHGC-8, PQBHGC-4 and PQBHGC-3 topologies to analyse their effectiveness in PV-driven BLDC motor applications. The simulation results show that the PQBHGC-3 topology is effective in comparison with other HG cell DC–DC converters in terms of efficiency, reduced ripples, etc. which is most suitable for PV-driven BLDC applications.

Findings – The simulation results have showed that the PQBHGC-3 gives better performance with minimum voltage ripple of 2V and current ripple of 0.4A which eventually reduces the ripples in the torque in a BLDC motor. Also, the efficiency for the suggested PQBHGC-3 for PV-based BLDC applications is the best with 99%.

The authors extend their appreciation to the Deanship of Scientific Research at King Khalid University for funding this work through General Research Project under Grant number (RGP.1/133/43).

Frontiers in Engineering and Built Environment
Vol. 4 No. 1, 2024
pp. 29-43
Emerald Publishing Limited
e-ISSN: 2634-2502
p-ISSN: 2634-2499
DOI 10.1108/FEBE-09-2022-0038

Originality/value – This study is the first of its kind comparing the different topologies of PQBHGC-1, PQBHGC-8, PQBHGC-4 and PQBHGC-3 topologies to analyse their effectiveness in PV-driven BLDC motor applications. This study suggests that the PQBHGC-3 topology is most suitable in PV-driven BLDC applications.

Keywords BLDC motor, PSO technique, PV arrays, Torque ripples, Quasi-Z-source converter

Paper type Research paper

1. Introduction

Investment in renewable energy sources has grown due to the recent rise in the price of fossil fuels and new legislation to decrease CO_2 emissions. Photovoltaic (PV) technologies are among the most popular sources of renewable energy, particularly in the United Arab Emirates, other Middle East countries, etc. (Revathi and Prabhakar, 2016). Irradiance and operating point affect PV output voltage, causing it to fluctuate. PVs' low unregulated voltage necessitates the use of a high ratio, high-efficiency DC–DC converter. Practical factors restrict the traditional boost converter's output voltage to a range of around six times the supply voltage. The typical boost converter must run at very high duty-cycle ratios in order to deliver a large output voltage. Low switching frequencies or ineffectively short off periods are imposed by extreme duty cycles. Because of the intense diode reverse-recovery current caused by short off times, the levels of electromagnetic interference will rise (Wu *et al.*, 2020).

During the course of the last decade, high-gain DC–DC converters have been the focus of a number of different research projects. It is possible to do this by positioning a high-gain (HG) cell in front of the output of the converter. It was decided to include three state switching cells as well as a voltage multiplier cell in order to increase the output voltage. However, the size of the converter is increased by the autotransformer (Sri Revathi and Mahalingam, 2018). Switching at zero voltage and switching at zero current are two options that have been proposed for the high step-up DC–DC converter that contains a voltage multiplier cell. The leakage inductance of the active clamp coupled inductor in the DC–DC converter has an effect on the voltage gain of the converter. This fault can be rectified by linking an inductor with a voltage multiplier cell, which results in a reduction in the high pulse current produced by the voltage doubler cell (Zhao *et al.*, 2011). A modified version of an interleaved boost converter is combined with a voltage multiplier module and a dual-connected inductor in order to provide current balancing in the main windings. The Villard, Heinrich Greinacher, Dickson and Cockcroft–Walton circuits were some of the first voltage multiplier designs to be used. These designs were used to generate high output voltage. A voltage lift circuit is coupled with the HGC-2 cell so that minimal voltage stress may be provided to the switches. In Shenkman *et al.* (2004), a significant voltage DC–DC converter is developed with the use of the Dickson multiplier cell HGC-3. In Shenkman *et al.* (2004), a Dickson cell and a switched coupled inductor are used to increase the voltage gain of the circuit. Diode reverse recovery losses are minimized by the recommended converter, which consists of an interleaved three-winding connected inductor and a voltage multiplier cell. An in-depth review of the HGC-3 cell's performance can be found in Navamani *et al.* (2017), which describes how the cell is paired with a conventional boost converter. When generating the extreme step-up DC–DC converter in Fardoun and Ismail (2010), the HGC-3 cell is employed as the generator. Navamani *et al.* (2017) incorporates a multiphase DC–DC converter as well as an HGC-7 cell in order to get rid of input current ripple and guarantee that the components of the converter share current adequately. In addition to this, the alternating phase shift control mechanism of the interleaved boost converter (Muhammad *et al.*, 2015) makes use of it. Chung-Ming Young and colleagues came up with a transformerless high step-up DC–DC converter that uses a Cockcroft–Walton (HGC-5) cell (Pan *et al.*, 2019). This converter was designed for use in direct current (DC) systems with very small inputs. It is recommended that you use the HGC-9, which is a bidirectional DC–DC converter. The HGC-3 is a quasi-Z-source network that is used in the production of step-up DC–DC converters. This network

is created by cascading quasi-Z-source cells. Positive output quadratic boost converter with high-gain converter (PQBHGC)-1, PQBHGC-8, PQBHGC-4 and PQBHGC-3 are evaluated and their performance is compared in this study. The comparison is done fairly.

Brushless direct current (BLDC) motors are gaining popularity in various applications like electric vehicles, traction locomotives, elevators, etc. due to their flexible speed control, high-speed torque, reliable operation, high efficiency and low maintenance (Lee *et al.*, 2005; Vijayakumar and Hemakumar, 2013). BLDC motors are similar like DC motors without brushes function, therefore the operational efficiency is more as compared with conventional DC motors. The BLDC motor draws rectangular currents, hence its back EMF is in trapezoidal shape. This wave shape influences the performance of BLDC motors. Improvements in BLDC control and performance can be attributed to the development of power electronic technology and high-speed digital signal processors. However, the non-rectangular phase currents lead to ripples in the torques which further affect the commutation of phase currents. Many researchers across the globe are finding solutions to overcome these problems in BLDC motors (Rahmani *et al.*, 2020; Kumar Sharma *et al.*, 2022).

A solar PV panel is a semiconductor material which generates the electricity through PV effect. PV array constitutes a number of solar PV panels, connected in series and parallel for large power generation. The PV arrays always operate in 85–90% of standard test conditions (STC) range due to the environmental facts. The efficiency of solar cells depends on the amount of sunlight and the electrical characteristics of the load falling on the solar panels. When the amount of sunlight changes and the high efficiency of the power line changes, i.e. the operation point of the system changes, to keep the power cable at a high level of efficiency, the maximum power point (MPP) has to be tracked. The maximum power point tracking (MPPT) is the procedure for locating this point and assessing the load characteristic with the best value. This load characteristic is known as the Maximum Power Point (MPP). Various MPPT techniques are available in the literature such as hill climbing, fuzzy logic controllers, neural networks, open-circuit and short-circuit methods, etc. (Su and Adams, 2001). These MPPT schemes are simple, less complex in implementation and require less sensors. In addition, these techniques work well under normal solar insolation conditions, however, the tracking performance is very highly influenced by drastic change in weather and partial shading conditions.

Real MPP is not always the same as the environment is varying continuously. Improved versions of the described algorithms are developed to find the optimum values within minimum time (Zhang and Lu, 2006). There are many methods in the literature for obtaining PI controller gain values. A mathematical model explaining how the acquired PI controller gain values were created was created in 1942 by Ziegler and Nichols when they were employed for Taylor Instruments. This method of tuning gives rugged response under dynamic conditions. Hence, various optimization techniques were introduced to get the optimal PI controller gain values. Fuzzy logic control has become an effective tool due to its stability, significant change of parameters, treatment of inequality and so on. However, it has drawbacks, such as (1) the lack of a maximum number selection method. Because the rules in this assessment include several factors, such as supervisor performance, compensation performance, selection of language variables and so on (Chen *et al.*, 2008; Shi *et al.*, 2010; Zhou *et al.*, 2020).

All the discussed topologies suggest that they have drawbacks of low voltage gain, high ripples in output voltage and current with low efficiency. With these drawbacks and issues in implementation and utilization of converters for PV-based BLDC applications, different high-gain converters are studied and analyzed. With a view to identify suitable converter for PV-based BLDC applications, the objectives are framed as follows:

(1) To model the HG cell, positive output quadratic boost high-gain converter (PQBHGC)-1, PQBHGC-8, PQBHGC-4 and PQBHGC-3 topologies both mathematically and in MATLAB/Simulink.

(2) To analyze the converters with their characteristics of gain, output voltage, output current ripples and efficiency.

(3) To compare the characteristics of PQBHGC-1, PQBHGC-8, PQBHGC-4 and PQBHGC-3 converters for suggesting the best converter for PV-based BLDC applications.

In this article, introduction and literature information related to the speed control of BLDC motor with various HG cell based DC–DC converters such as PQBHGC-1, PQBHGC-8, PQBHGC-4 and PQBHGC-3 converters with PV system are described in Section 1. The description on PV-based BLDC motor drive with quasi-Z-source converter and steady-state analysis of PQBHGC-1,8, 4 and 3 types of converters are presented in Section 2. Analysis on the impact of partial shading on solar panels is presented in Section 3. The closed-loop control techniques of PI with particle swarm optimization (PSO) are illustrated in Section 4. Section 5 discusses the simulation results of PQBHGC-1,8, 4 and 3 types of converters for PV-driven BLDC applications and followed by conclusions in Section 6.

2. PV-based BLDC motor drive with quasi-Z-source converter

a. Description of high-gain q-ZSC

The block diagram of proposed system is shown in Figure 1. It consists of two PV panels connected in parallel, a high-gain q-ZSC boost converter and a BLDC motor. The operation of the proposed system is configured to investigate the speed control and ripples under normal solar insolation changes and partial shading conditions.

b. Steady-state analysis of PQBHGC-1, PQBHGC-3, PQBHGC-4 and PQBHGC-8

In order to get a more in-depth understanding of the PQBHGC, a few different topologies have been analyzed, and the steady-state analysis of those topologies has been performed in order to figure out their voltage gain using an HG cell. Figure 2 presents the schematic circuit of PQBHGC-1, 3, 4 and 8 HG cell DC–DC converters (Navamani *et al.*, 2017).

c. Operating modes of PQBHGC-1 and PQBHGC-8

Figure 3 (a) and 3 (b) shows the operation modes of a positive output quadratic boost converter with high-gain PQBHGC-1 and PQBHGC-8. (b) (Navamani *et al.*, 2017). To simplify the analysis, a single HG cell is considered for high-gain q-ZSC. The current through the inductor and voltage across the capacitor are measured during the on and off phases to perform steady-state analysis.

In modes 1 and 2, the voltage across the inductor is expressed as (Navamani *et al.*, 2017)

$$U_{L1} = U_g;\ U_{L1} = U_g - U_c; \tag{1}$$

$$U_{L2} = U_c;\ U_{L2} = U_c - U_{cm} \tag{2}$$

$$U_{Lo} = 2U_{cm} - U_0;\ U_{Lo} = U_{cm} - U_o \tag{3}$$

putting the volt-second balance into Equations 1, 2 and 3

$$U_c = \frac{U_g}{1-D};\ U_{cm1} = U_{cm2} = \frac{U_g}{(1-D)^2} \tag{4}$$

Now, apply voltage conversion ratio as follows:

$$\frac{U_0}{U_g} = \frac{(1-D)}{(1-D)^2} \tag{5}$$

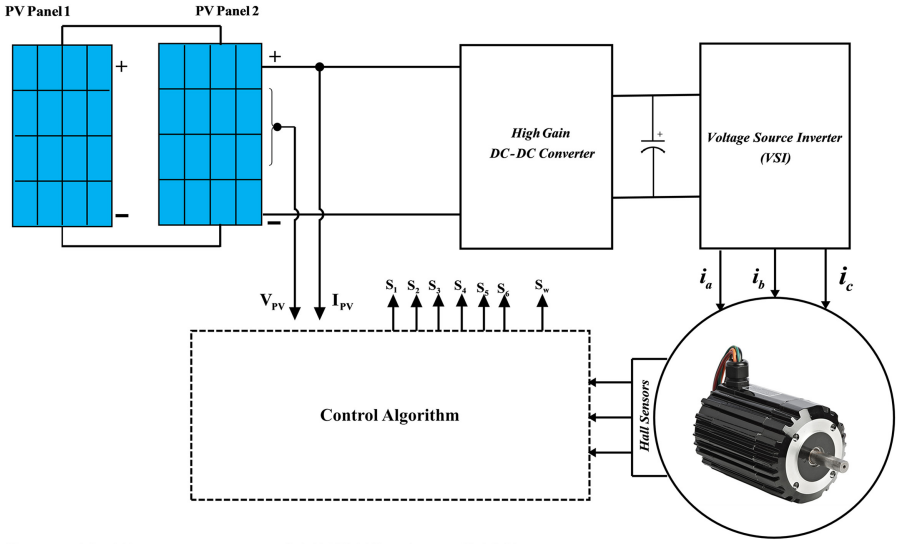

Source(s): Figure courtesy of ZMS Elbarbary (2023)

Figure 1.
High-gain DC–DC converter for PV-driven BLDC motor applications

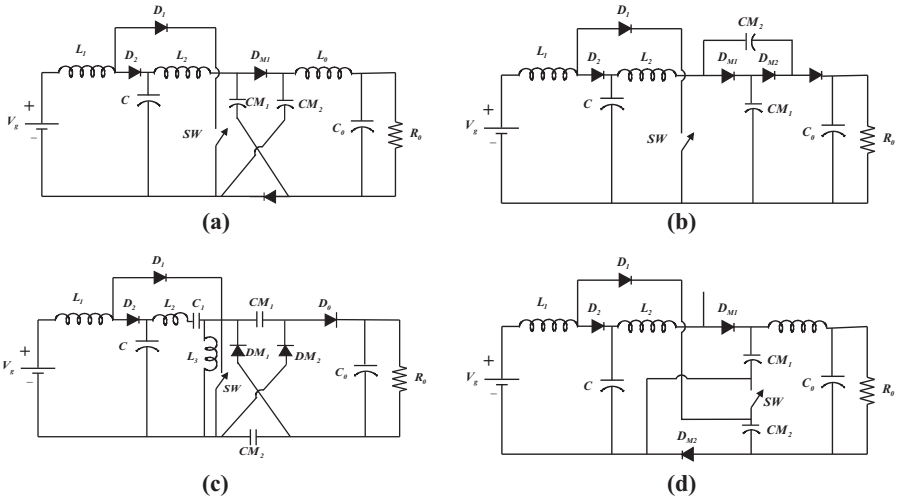

Source(s): Figure courtesy of Navamani (2017)

Figure. 2.
Various HG cell DC–DC converters (a) PQBHGC-1 (b) PQBHGC-3 (c) PQBHGC-4 (d) PQBHGC-8

d. Operating modes of PQBHGC-3

Quadratic boost converter with a positive output obtained from the Dickson multiplier cell, HG cell 3 is shown in Figure 4 (Navamani *et al.*, 2017). For the sake of simplicity, just one cell is taken into account for the steady-state analysis, and the modes of operation are shown in Figure 4 (b). In modes 1 and 2, voltage across the inductor is expressed as

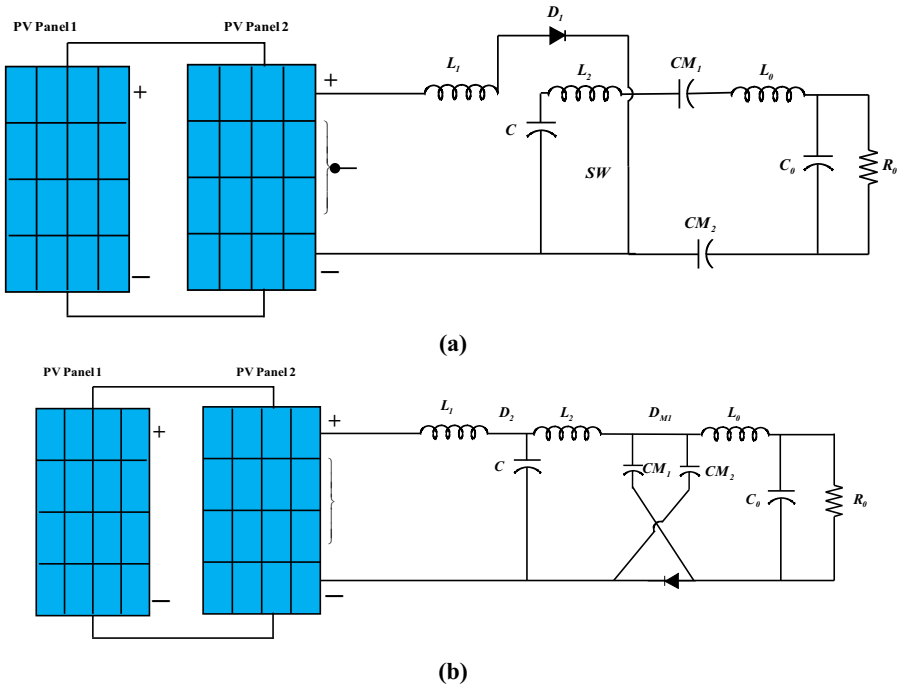

Figure 3.
Modes of operation (a) Mode-1 (b) Mode-2

Source(s): Figure courtesy of ZMS Elbarbary (2023)

$$U_{L1} = V_g;\ U_{L1} = V_g - V_c \tag{6}$$

$$U_{L2} = V_c;\ U_{L2} = V_c - V_{cm} \tag{7}$$

$$V_{cm1} = V_{cm2};\ V_o = V_{cm1} + V_{cm2} \tag{8}$$

Now, apply volt-second balance formula to the above equations.

$$U_c = \frac{V_g}{(1-D)};\ V_{CM1} = \frac{V_g}{(1-D)^2} \tag{9}$$

Then, the voltage conversion ratio for *PQBHGC-3* is written as follows:

$$\frac{V_o}{V_g} = \frac{2}{(1-D)^2} \tag{10}$$

e. Operating modes of PQBHGC-4

The steady-state analysis of *PQBHGC*-4 is made by analyzing the power switch on/off of the PQBHGC-4 in mode-1 and mode-2 as shown in Figure 5(a) and 5(b), respectively (Navamani *et al.*, 2017).

$$U_{L1} = V_g;\ U_{L1} = V_g - U_c; \tag{11}$$

$$U_{L2} = U_c;\ U_{L2} = U_c - U_{cm}; \tag{12}$$

$$U_{L3} = U_{cm};\ U_{L3} = 2U_{cm} - U_0; \tag{13}$$

Now, apply volt-second balance formula to the above equations.

$$U_c = \frac{V_g}{(1-D)};\ U_{cm} = \frac{V_g}{(1-D)^2} \tag{14}$$

Then, the voltage conversion ratio for *PQBHGC-4* is written as follows:

$$\frac{V_o}{V_g} = \frac{2-D}{(1-D)^2} \tag{15}$$

3. Maximum power point tracking and control methodologies

3.1 Analysis on the impact of partial shading on solar panels

Understanding the impact of partial shadowing on the PV system under PSC was the goal of the investigation. Due to obstacles such as passing clouds, dust getting into the PV system, etc., the PV array experiences PSC. As a result, the insolation levels received by various solar panels vary. This reduces the effectiveness of the system, and if it persists, it might cause actual system damage. This formula is used to determine the effective insolation:

$$S_E = (1 - K)S \tag{16}$$

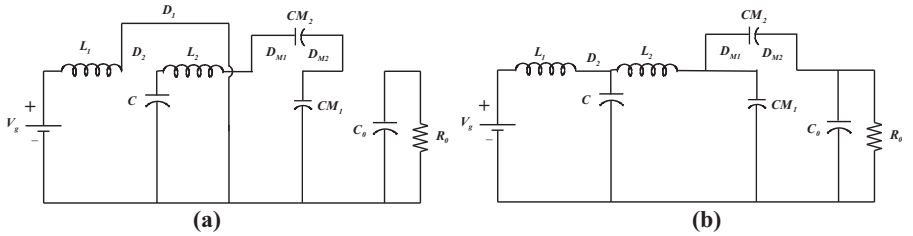

Source(s): Figure courtesy of Navamani (2017)

Figure 4.
Operating modes of (PQBHGC-3)

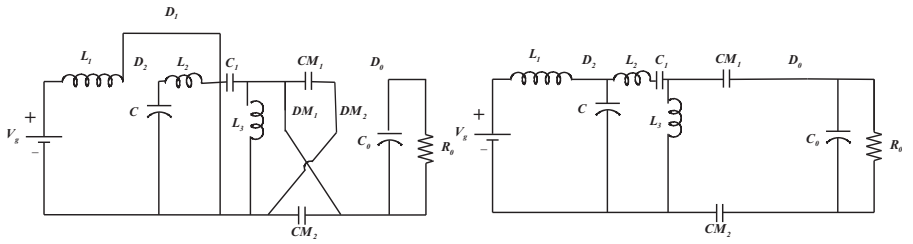

Source(s): Figure courtesy of Navaman (2017)

Figure 5.
Operating modes of (PQBHGC-4)

where K represents the panel shading ratio, S represents the insolation level on the solar panel's unshaded area and SE represents the effective insolation on each solar panel. The percentage of a solar panel's shaded area to its overall area is known as the shading ratio. Two parallel panels that are partially shaded are joined together for analytical purposes. Figure 6 shows the two PV panels connected in parallel. The solar PV module's output current is provided with

$$I = I_{ph} - I_D\left[e^{\left\{q\left(U_{pv}+I_{ph}R_s\right)/N_sAB_kT\right\}} - 1\right] - \frac{U_{pv} + I_{pv}R_sN_s}{N_sR_{sh}} \quad (17)$$

Due to the differing insolation levels experienced by the two parallel-connected solar panels, Ipv1 and Ipv2 currents are developed. If the output PV current is greater than the produced photo-generated current Ipv1 (Iph).

Figure 7 of PV curve features two distinct MPPs, one of which is local MPP and the other is GMPP. If N PV panels are connected in series and parallel, finding the GMPP is fairly difficult. As a result, this work proposes a quasi-Z-source DC–DC converter using a PSO-based MPPT algorithm to address the problem.

In order to improve the overall functionality of the system, the GMPP tracking schemes have to be designed with the criteria listed below.

(1) Accurately tracking global MPP in a timely manner while avoiding falling into local MPP

(2) The possibility of its implementation

(3) The fact that, when linked to the grid, it is efficient and cuts down on noise

a. Closed-loop speed control of BLDC motor

This section describes the acquisition of PI on MATLAB /Simulink, which shows the feedback speed control of BLDC motor behavior. The speed control is achieved by PI control effectively, but nonlinearity occurs due to saturation element. Mainly PI controllers are used to remove critical controls steady-state error. The side effect is called the integrator. This can

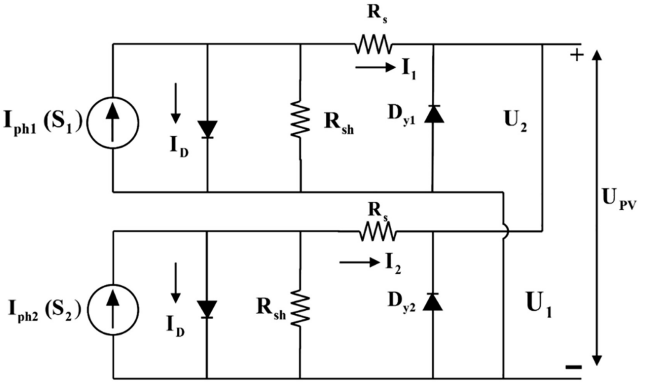

Source(s): Figure courtesy of ZMS Elbarbary (2023)

Figure 6.
Circuit diagram for parallel connection of two PV panels

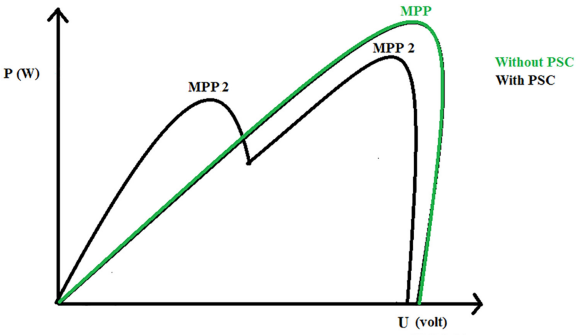

Source(s): Figure courtesy of ZMS Elbarbary (2023)

Figure 7.
Characteristics of the power and voltage delivered by solar arrays

happen if there are significant changes in the set points. This effect results in higher overshoot and more settling time.

b. Particle swarm optimization technique

PSO is used to solve the multi-behavioral characteristics of any system by work population-based function. This was invented by Eberhart and Kennedy. Due to versatile characteristics by solving the nonlinearity functions of the system when it under does transient behavior.

The PSO is implemented to have effective speed control of the BLDC motor. The BLDC motor has been very popular due to variety of the speed range. PSO has proven to be very effective in solving nonlinearity, differentiation, function, multipurpose and multidimensional problems. This PSO is developed for the speed control of BLDC motor applications to improve the tuning of PI controller. The following equation shows the particle position and position of particles:

$$x^{i}_{k+1} = \chi x^{i}_{k} + \lambda_1 . b_1 \left(q^{i}_{Lbest} - y^{i}_{k} \right) + \lambda_2 . b_2 \left({q_{gbest}}^{i} - y^{i}_{k} \right) \tag{18}$$

$$y^{i}_{k+1} = y^{i}_{k} (1 - \lambda_2) + \lambda_2 q_{gbest} + \eta\beta \tag{19}$$

where k and i are the no. of iterations participated by the particle. q^{i}_{Lbest} is the local best and q^{i}_{Gbest} is the global best obtained by the particles. The particle position and velocity are y^{i}_{k} and x^{i}_{k}, respectively. The updated position and velocities of particle are y^{i}_{k+1} and y^{i}_{k+1}, respectively. The b_1 and b_2 are the random numbers which are in the range of [-1, 1]. The flow chart of PSO technique is shown in Figure 8.

4. Simulation results and discussion

The proposed system as shown in Figure 1 is developed in MATLAB/Simulink environment. The system parameters used for simulation study are tabulated in Appendix. The system consists of PV array, various PQBHGC DC–DC converters, three-phase inverters, BLDC motor and PSO-based PI controller.

The performance of PQBHGC-1, PQBHGC-8, PQBHGC-4 and PQBHGC-3 high-gain topologies are simulated under steady solar input conditions in Figure 9(a) – 9(d), respectively. The low voltage DC side of converters is boosted to high voltages to run the BLDC motor. The change in solar insolation of 1000 W/m^2 and 500 W/m^2 is observed from

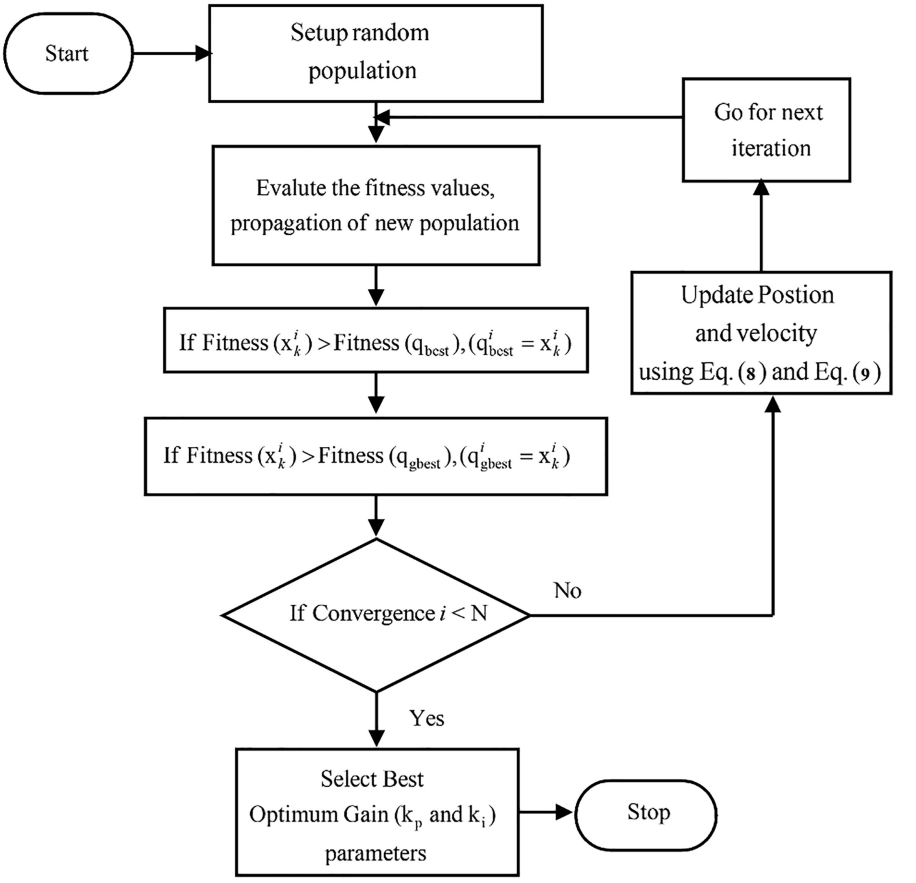

Figure 8.
Flowchart of PSO

Source(s): Figure courtesy of ZMS Elbarbary (2023)

$t = 1$s to $t = 2$s, when solar insolation changes, the PSO MPPT control techniques track the MPP to extract the optimal power from the solar panel. It is observed from Figure 9(a) – 9(d) that the PQBHGC-3 gives better performance with minimum voltage ripples of 2 V and 0.4 A of current ripple with high efficiency of 99%. A fair comparison is made between characteristics of various HG cell based DC–DC converter topologies. Output voltage, current, efficiency, voltage and current ripples are evaluated and compared as tabulated in Table 1. It is also observed the performance of BLDC motor under this condition is shown in Figure 10, and back EMF of phase-a, phase-b and phase-c also phase currents are shown in Figure 11.

The rotation speed and reference speed are compared which generates speed error. This speed error is given to generate a high-speed PI controller current reference line. In addition, the current line is current, and a reference flow is added to generate the current error. The generated error goes to hysteresis current controller and generates the switching signals for BLDC inverter.

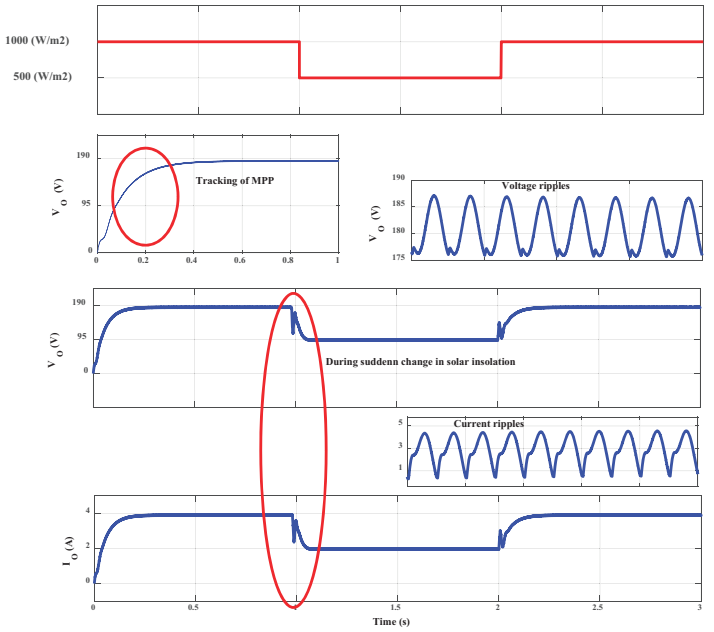

Figure 9.
Performance of HG cell DC–DC converter topologies (a) PQBHGC-1 (b) PQBHGC-8 (c) PQBHGC-4 (d) PQBHGC-3

(*continued*)

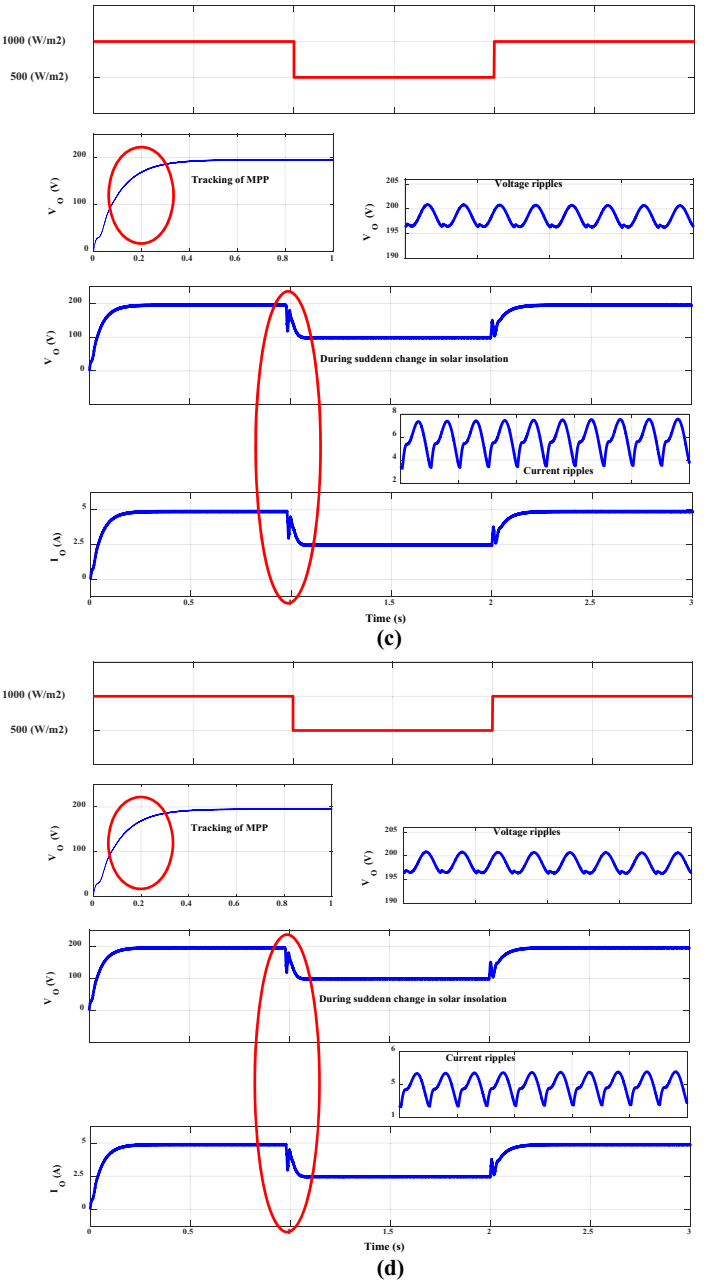

Figure 9.

Source(s): Figure courtesy of ZMS Elbarbary (2023)

5. Conclusion

This paper presents various HG cell DC–DC converters such as PQBHGC-1, PQBHGC-8, PQBHGC-4 and PQBHGC-3 that are tested for the speed control of PV-based BLDC motor

Topology	U_{out} (V)	I_{out} (A)	P_{out} (W)	Efficiency (%)	Ripples U_{out} (V)	Ripples I_{out} (A)
PQBHGC-1	182	4.2	764.4	76.44	12	1.2
PQBHGC-8	187	4.5	841.5	84.15	9	0.9
PQBHGC-4	195	4.5	877.5	87.75	6	0.7
PQBHGC-3	198	5	990	99.0	2	0.4

Source(s): Table courtesy of ZMS Elbarbary, 2023

Table 1. Performance comparison of various HG cell based DC–DC converters

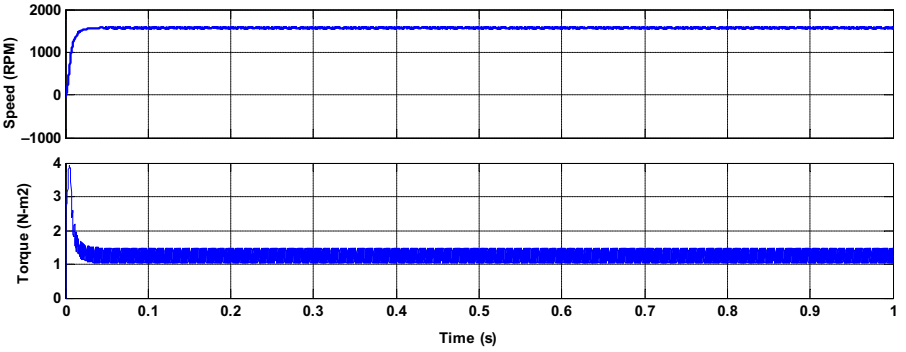

Source(s): Figure courtesy of ZMS Elbarbary (2023)

Figure 10. BLDC motor speed and torque curve under steady-state condition

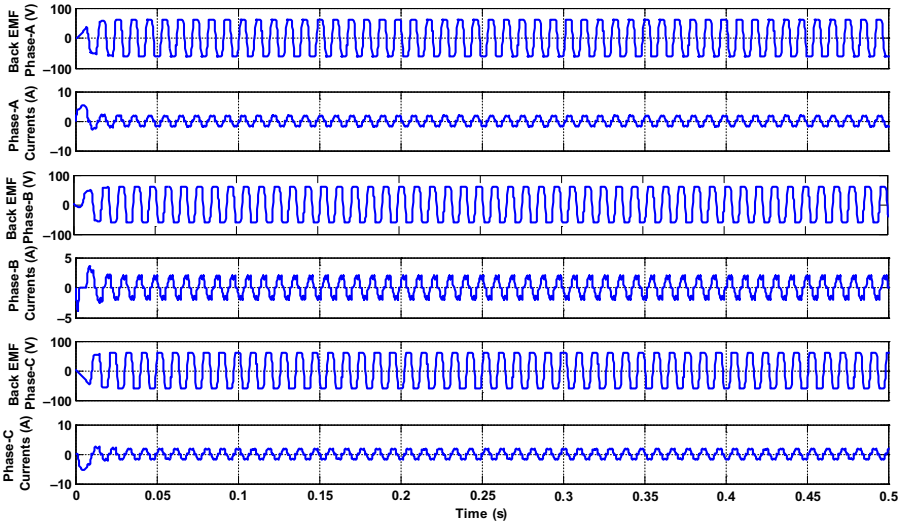

Source(s): Figure courtesy of ZMS Elbarbary (2023)

Figure 11. Performance of BLDC motor under steady-state condition of solar insolation

with PSO-based closed-loop control technique under normal solar insolation and partial shading conditions. BLDC motor becomes very popular in electric vehicle applications due to its wide range speed, high efficiency, etc. The speed control is achieved by closed-loop control implemented with PI controllers because of its ease of implementation, low cost, etc. A PSO method is opted for this system to calculate the optimum PI controller gain parameters under steady-state and dynamic changing conditions. The entire proposed system is designed in MATLAB/Simulink and tested under various scenarios of weather tested the various HG cell boost converters. The simulation results have shown that the PQBHGC-3 gives better performance with minimum voltage ripple of 2 V and current ripple of 0.4 A which eventually reduces the ripples in the torque in BLDC motor. Also, the efficiency for the suggested PQBHGC-3 for PV-based BLDC application is the best with 99%.

References

Chen, W., Xia, C.L. and Xue, M. (2008), "A torque ripple suppression circuit for brushless DC motors based on power dc/dc converters", *Proceeding IEEE Industrial Electronics and Applications, Conference*, pp. 1453-1457.

Fardoun, A.A. and Ismail, E.H. (2010), "Ultra step-up DC–DC converter with reduced switch stress", *IEEE Transactions on Industry Applications*, Vol. 46 No. 5, pp. 2025-2034.

Kumar Sharma, S., Kumar Gupta, S. and Gali, V. (2022), "Design and performance analysis of photovoltaic powered DC motor drive under non-uniform insolation conditions", *2022 First International Conference on Electrical, Electronics, Information and Communication Technologies (ICEEICT)*, pp. 1-6.

Lee, H.-W., Kim, T.-H. and Ehsani, M. (2005), "Practical control for improving power density and efficiency of the BLDC generator", *IEEE Translation Power Electronic*, Vol. 20 No. 1, pp. 192-199.

Muhammad, M., Armstrong, M. and Elgendy, M.A. (2015), "A nonisolated interleaved boost converter for high-voltage gain applications", *IEEE Journal of Emerging and Selected Topics in Power Electronics*, Vol. 4 No. 2, pp. 352-362.

Navamani, D., Vijayakumar, K. and Jegatheesan, R. (2017), "Study on high step-up DC-DC converter with high gain cell for PV applications", *Procedia Computer Science*, Vol. 115, pp. 731-739.

Pan, X., Li, H., Liu, Y., Zhao, T., Ju, C. and Rathore, A.K. (2019), "An overview and comprehensive comparative evaluation of current-fed-isolated-bidirectional DC/DC converter", *IEEE Transactions on Power Electronics*, Vol. 35 No. 3, pp. 2737-2763.

Rahmani, F., David, Q., Agarwal, T. and Barzegaran, M. (2020), "Speed control of brushless DC motor by DC-DC boost and buck converters using GaN and SiC transistors for implementing the electric vehicles".

Revathi, B.S. and Prabhakar, M. (2016), "Non isolated high gain DC-DC converter topologies for PV applications–A comprehensive review", *Renewable and Sustainable Energy Reviews*, Vol. 66, pp. 920-933.

Shenkman, A., Berkovich, Y. and Axelrod, B. (2004), "Novel AC-DC and DC-DC converters with a diode-capacitor multiplier", *IEEE Transactions on Aerospace and Electronic Systems*, Vol. 40 No. 4, pp. 1286-1293.

Shi, T., Guo, Y., Song, P. and Xia, C. (2010), "A new approach of minimizing commutation torque ripple for brushless dc motor based on dc-dc converter", *IEEE Translation Induction Electronic*, Vol. 57 No. 10, pp. 3483-3490.

Sri Revathi, B. and Mahalingam, P. (2018), "Non-isolated high gain DC–DC converter with low device stress and input current ripple", *IET Power Electronics*, Vol. 11 No. 15, pp. 2553-2562.

Su, G.J. and Adams, D.J. (2001), "Multilevel DC-link inverter for brushless permanent magnet motors with very low inductance", *Conference Record IEEE-IAS Annual Meeting*, pp. 829-834.

Vijayakumar, G. and Hemakumar, K. (2013), "Development of low cost high efficient DC-DC converter for photovoltaic system with fast converging MPPT algorithm", *2013 International conference on Renewable energy and Sustainable energy (ICRESE)*, IEEE, pp. 98-104.

Wu, X., Yang, M., Zhou, M., Zhang, Y. and Fu, J. (2020), "A novel high-gain dc-dc converter applied in fuel cell vehicles", *IEEE Transactions on Vehicular Technology*, Vol. 69 No. 11, pp. 12763-12774.

Zhang, X.F. and Lu, Z.Y. (2006), "A new BLDC motor drives method based on BUCK converter for torque ripple reduction", *Proceding IEEE Power Electronics and Motion Control Conference*, pp. 1-4.

Zhao, Y., Li, W. and He, X. (2011), "Single-phase improved active clamp coupled-inductor-based converter with extended voltage doubler cell", *IEEE Transactions on Power Electronics*, Vol. 27 No. 6, pp. 2869-2878.

Zhou, Q., Shu, J., Cai, Z., Han, C. and Zhang, Y. (2022), "Optimal duty cycle method to suppress the commutation torque ripple of brushless DC motor in braking mode", *Journal of Electrical Engineering and Technology*, Vol. 17 No. 3, pp. 1731-1739.

Appendix

The appendix for this article can be found online.

Corresponding author

Zakaria Mohamed Salem Elbarbary can be contacted at: albrbry@kku.edu.sa